Prediction of Turbulent Heat Transfer Using Hybrid LES-RANS

L. Davidson
Division of Fluid Dynamics
Department of Applied Mechanics
Chalmers University of Technology
SE-412 96 Göteborg
http://www.tfd.chalmers.se/~lada

April 29, 2007

1 Introduction

Heat transfer is important in many industrial applications. In some applications – such as heat exchangers of all kind – the aim is to maximize the heat transfer across a surface. On the other hand, on gas turbines blades, in exhaust piping systems in vehicles, in piping systems carrying hot water – the aim is to minimize the heat transfer in order to minimize losses. Often the object is to reduce the thermal load. High thermal load causes thermal fatigue which may result in fatigue crack initiation and propagation which eventually may lead to structural failure. High temperature fluctuations are often more damaging than high mean temperatures. Fluctuating wall temperatures act as boundary conditions when predicting heat transfer in the solid material adjacent to the hot/cold fluid. Hence, without accurate predicted wall temperatures, there is no hope to be able to predict the risk of thermal fatigue due to fluctuating thermal load. As is shown in the present work, the temperature fluctuations are indeed very large.

In traditional CFD (i.e. RANS[1]) of fluid flow and heat transfer, the turbulent fluctuations (both velocity and temperature) are modelled. To achieve accurate predictions of the mean fluid flow and temperature, accurate prediction of the turbulent fluctuations are needed.

[1]RANS=Reynolds-Averaged Navier-Stokes

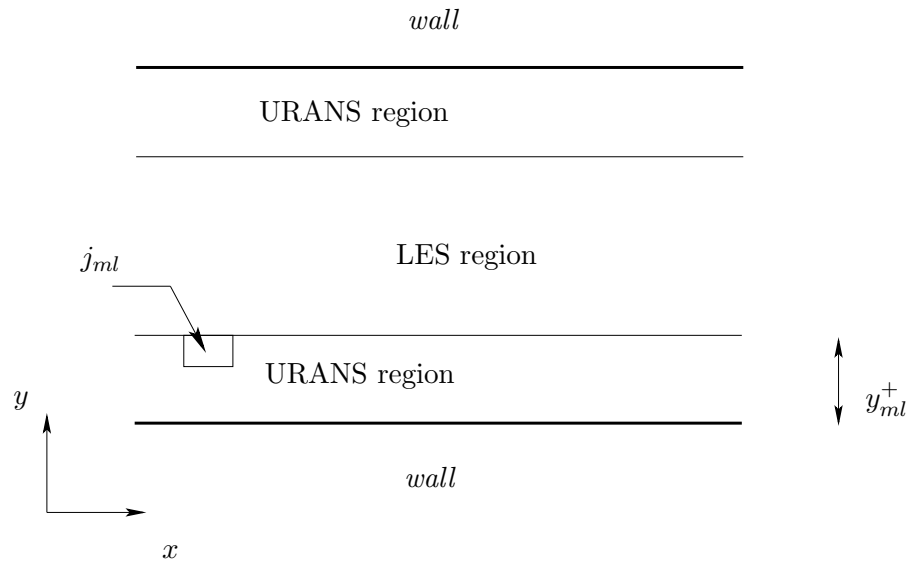

Figure 1: The LES and URANS regions. The interface is located at $y^+ = y^+_{ml}$ and the number of cells in the URANS region in the wall-normal direction is j_{ml}.

2 Numerical details

2.1 The Momentum Equations

The Navier-Stokes equations with an added turbulent/SGS viscosity read

$$\begin{aligned} \frac{\partial \bar{U}_i}{\partial t} + \frac{\partial}{\partial x_j}\left(\bar{U}_i\bar{U}_j\right) &= \delta_{1i} - \frac{1}{\rho}\frac{\partial \bar{P}}{\partial x_i} + \frac{\partial}{\partial x_j}\left[(\nu+\nu_T)\frac{\partial \bar{U}_i}{\partial x_j}\right] \\ \frac{\partial \bar{U}_i}{\partial x_i} &= 0 \\ \frac{\partial \bar{T}}{\partial t} + \frac{\partial}{\partial x_j}\left(\bar{U}_j\bar{T}\right) &= \frac{\partial}{\partial x_j}\left[\left(\frac{\nu}{Pr} + \frac{\nu_T}{Pr_t}\right)\frac{\partial \bar{T}}{\partial x_j}\right] \end{aligned} \tag{1}$$

where $\nu_T = \nu_t$ (ν_t denotes the turbulent RANS viscosity) close to the wall for $y \leq y_{ml}$, otherwise $\nu_T = \nu_{sgs}$, see Fig. 1. The laminar and turbulent Prandtl number are set to 0.72 and 0.9, respectively. The turbulent viscosity, ν_T, is computed from an algebraic turbulent length scale, see Table 1, and a transport equation is solved for k_T. The density is set to one in all simulations. For channel flow, a driving constant pressure gradient, δ_{1i}, is included in the streamwise momentum equation.

2.2 Hybrid LES–RANS

A one-equation model is employed in both the URANS region and the LES region (see Fig. 1) and reads

$$\frac{\partial k_T}{\partial t} + \frac{\partial}{\partial x_j}(\bar{U}_j k_T) = \frac{\partial}{\partial x_j}\left[(\nu + \nu_T)\frac{\partial k_T}{\partial x_j}\right] + P_{k_T} - C_\varepsilon \frac{k_T^{3/2}}{\ell}$$
$$P_{k_T} = -\tau_{ij}\bar{S}_{ij}, \quad \tau_{ij} = -2\nu_T \bar{S}_{ij}$$

where $\nu_T = ck^{1/2}\ell$. The location at which the switch is made from URANS to LES is called the interface and is located at y_{ml} from each wall. In the inner region ($y \leq y_{ml}$) k_T corresponds to RANS turbulent kinetic energy, k; in the outer region ($y > y_{ml}$) it corresponds to subgrid-scale kinetic turbulent energy, k_{sgs}. The model constants are different in the two regions, see Table 1. No special treatment is applied in the equations at the matching plane except that the form of the turbulent viscosity and the turbulent length scale are different in the two regions. $k_T = 0$ at the walls. Greater detail is given in Davidson & Billson (2006).

2.3 The Numerical Method

An incompressible, finite volume code is used (Davidson & Peng, 2003). For space discretization, central differencing is used for all terms except for the convection term in the k_T equation for which the hybrid central/upwind scheme is employed. The Crank-Nicolson scheme is used for time discretization of all equations. The numerical procedure is based on an implicit, fractional step technique with a multigrid pressure Poisson solver (Emvin, 1997) and a non-staggered grid arrangement.

3 Results.

In the present work, unsteady simulations (DNS and hybrid LES-RANS) are carried out for fluid flow and heat transfer in a channel at two different Reynolds numbers and for an asymmetric diffuser.

	URANS region	LES region
ℓ	$2.5n[1 - \exp(-0.2k^{1/2}n/\nu)]$	$\ell = \Delta$
ν_T	$2.5k^{1/2}n[1 - \exp(-0.014k^{1/2}n/\nu)]$	$0.07k^{1/2}\ell$
C_ε	1.0	1.05

Table 1: Turbulent viscosities and turbulent length scales in the URANS and LES regions. n denotes the distance to the nearest wall. $\Delta = (\delta V)^{1/3}$

.

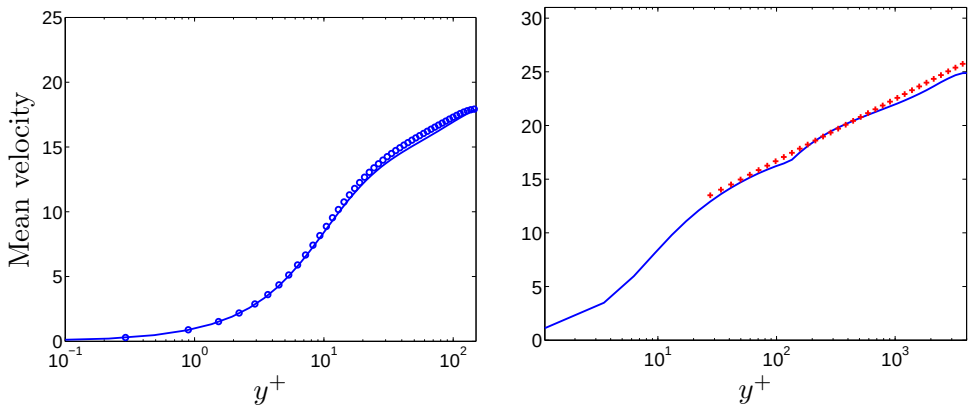

(a) DNS, $Re = 150$.

(b) Hybrid LES-RANS, $Re = 4000$.

Figure 2: Streamwise velocities. $\langle \bar{U} \rangle$ profiles. $\circ$: DNS at $Re_\tau = 180$ by Moser *et al.* (1999); $+$: $2.5 \ln(y^+) + 5.2$;

3.1 Channel Flow Simulations.

The grid used in hybrid LES-RANS is coarse, in order to investigate how well hybrid LES-RANS works on such grids. The Reynolds number is defined as $Re_\tau = u_\tau \delta / \nu = 4000$, where δ denotes channel half width and u_τ denotes friction velocity related to the driving pressure gradient. A $64 \times 80 \times 64$ mesh (x, streamwise; y, wall-normal; z, spanwise) is used. The size of the computational domain is $x_{max} = 6.4$, $y_{max} = 2\delta = 2$, $z_{max} = 3.2$. $\langle \cdot \rangle$ denotes time, spanwise and streamwise averaging.

For the DNS simulation, the Reynolds number is $Re_\tau = 150$. The mesh has $128 \times 96 \times 128$ cells and the extent of the domain is $4\pi \times 2 \times 2\pi$. In DNS, the turbulent viscosity is set to zero and the k_T equation is not solved.

For both $Re_\tau = 4000$ and $Re_\tau = 150$ the temperature is set to one at the lower (south) wall and 0 at the upper (north) wall, i.e. $T_s = 0$ and $T_n = 1$.

The DNS mean velocity ($Re_\tau = 150$) is in Fig. 2a compared to DNS of Moser *et al.* (1999) and as can be seen the agreement is very good. The agreement for the stresses is also very good (not shown). Hence the DNS results are here consider to be exact. The velocity profile for the hybrid LES-RANS results ($Re_\tau = 4000$) agrees fairly well with the logarithmic profile, as can be seen in Fig. 2b. Forcing is used at the interface (Davidson & Billson, 2006). A small jump is seen in the velocity profile at the interface between the URANS and the LES region.

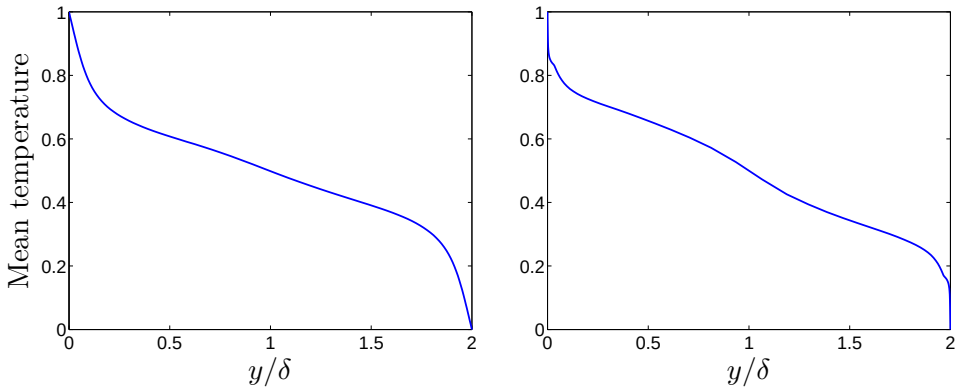

(a) DNS, $Re = 150$. (b) Hybrid LES-RANS, $Re = 4000$.

Figure 3: Channel flow. Mean temperature.

3.1.1 Heat transfer

The mean temperature profiles are shown in Fig. 3 and as expected the boundary layer is much thinner for $Re_\tau = 4000$ than for $Re_\tau = 150$ (no experimental temperature data exist for this case). The Nusselt number based on δ and $\Delta T = 1$ is $Nu = 2.75$ for the former case and $Nu = 50.5$ for the latter, and thus the ratio is 18.4. According to experimental correlations the Nusselt number should vary with bulk Reynolds number as $Re^{4/5}$ (Incropera & DeWitt, 1996), which gives $(101\,000/2\,300)^{4/5} = 20.6$ and hence the predictions and the correlations are in reasonable agreement. The actual Nusselt numbers given by the correlations are some 50% larger than the predicted values for both Reynolds numbers.

The resolved normal stresses are presented in Fig. 4. Note that the streamwise stress is up to almost one order of magnitude larger than the wall-normal stress. This is also the case for the ratio of the streamwise and wall-normal heat flux, $\langle u't' \rangle / \langle v't' \rangle$, see Fig. 5. The spanwise spanwise heat flux, $\langle w't' \rangle$, is zero for the same reason as the spanwise Reynolds stresses, $\langle u'w' \rangle$ and $\langle v'w' \rangle$: their production terms are zero because $\bar{V} = \bar{W} = \partial/\partial z = 0$. The resolved wall-normal heat flux is constant in the central region of the channel for both Reynolds numbers, because the time-averaged temperature equation reads

$$0 = \frac{\nu}{Pr} \frac{\partial^2 \langle \bar{T} \rangle}{\partial y^2} + \frac{\partial}{\partial y} \left(\frac{\nu_t}{Pr_t} \frac{\partial \langle \bar{T} \rangle}{\partial y} \right) - \frac{\partial \langle v't' \rangle}{\partial y} \tag{2}$$

For $Re_\tau = 150$ (DNS), the second term is zero and it is small in the central region for $Re_\tau = 4000$. The first term is negligible everywhere except very close to the wall. Hence, the y-derivative of $\langle v't' \rangle$ must be zero for

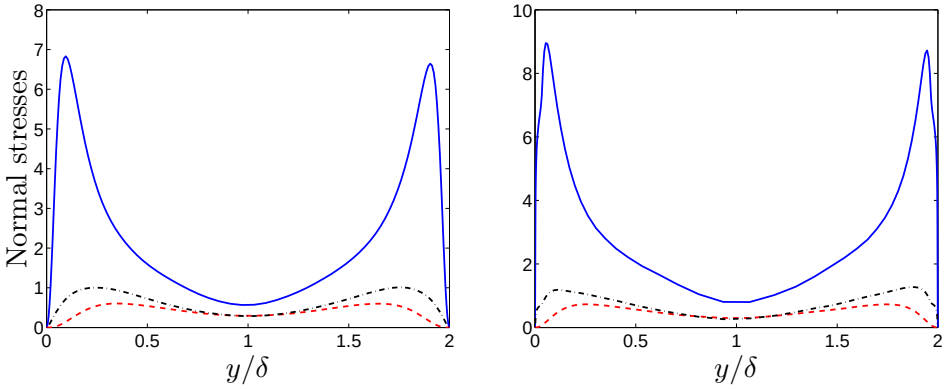

(a) DNS, $Re = 150$. (b) Hybrid LES-RANS, $Re = 4000$.

Figure 4: Channel flow. Resolved normal stresses. —— : $\langle u'^2\rangle/u_\tau^2$; - - - : $\langle v'^2\rangle/u_\tau^2$; - - - : $\langle w'^2\rangle/u_\tau^2$.

a large part of the channel. Davidson *et al.* (2003) includes a discussion on why stresses and heat fluxes vary as they do. Note that inner scaling has been used both for the stresses and the heat fluxes, i.e. they have been normalized with the friction velocity, u_τ and the friction temperature $t_\tau = |-\nu/(u_\tau Pr)(\partial\bar{T}/\partial y)_w|$ defined at the walls. Inner scaling is particularly relevant when we are dealing with heat transfer, since the wall heat indeed takes place at the walls.

Figure 6 presents the resolved temperature fluctuations. As can be seen they are very large. They are actually larger than the streamwise fluctuations. For both Reynolds numbers it can be seen that a peak in $\langle t'^2\rangle$ appears in the center. This can be explained by the production term in the transport equation for $\langle t'^2\rangle$ which reads (Davidson *et al.*, 2003)

$$P_{tt} = -\langle v't'\rangle \frac{\partial\langle\bar{T}\rangle}{\partial y} \tag{3}$$

The temperature gradient has a small negative peak at the center (this is visible in Fig. 3b) which together with negative $\langle v't'\rangle$ creates the peak in $\langle t'^2\rangle$.

As mentioned in the introduction, accurate prediction of the temperature fluctuations at the walls are crucial for accurate prediction of heat conduction in the solid part of the domain. The fluctuating wall shear stress and wall heat flux

$$\tau'_{w,RMS} = \nu\frac{\partial u'_{RMS}/u_\tau}{\partial y}, \quad q'_{w,RMS} = \frac{\nu}{Pr}\frac{\partial t'_{RMS}/t_\tau}{\partial y} \tag{4}$$

are 0.29 and 0.34, respectively, for $Re_\tau = 4000$. For $Re_\tau = 150$, $\tau'_{w,RMS} = 0.36$ and $q'_{w,RMS} = 0.39$. Thus the fluctuating wall shear stress and wall

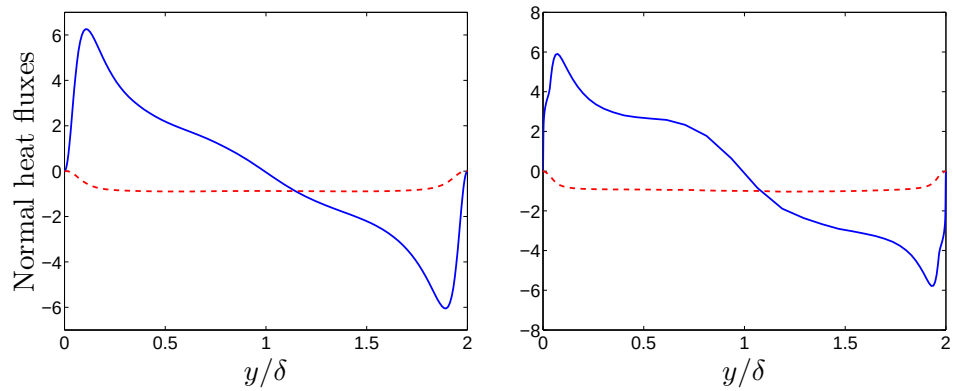

(a) DNS, $Re = 150$. (b) Hybrid LES-RANS, $Re = 4000$.

Figure 5: Channel flow. Resolved normal stresses. —— : $\langle u't' \rangle / (u_\tau t_\tau)$; - - - : $\langle v't' \rangle / (u_\tau t_\tau)$.

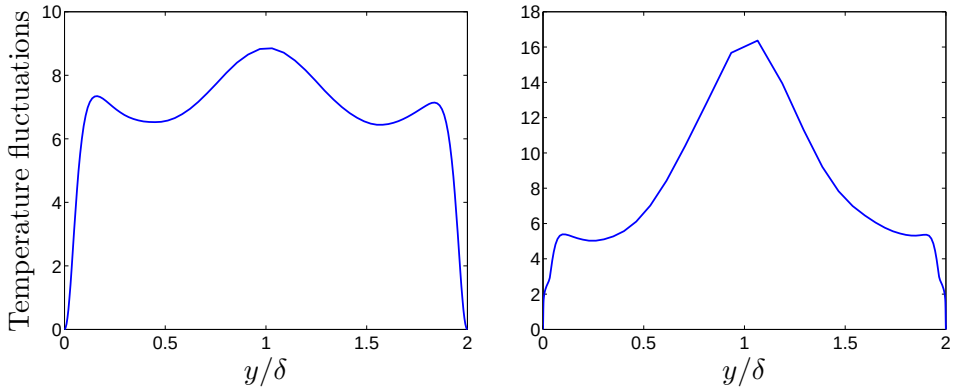

(a) DNS, $Re = 150$. (b) Hybrid LES-RANS, $Re = 4000$.

Figure 6: Channel flow. Temperature fluctuations, $\langle t'^2 \rangle / t_\tau^2$.

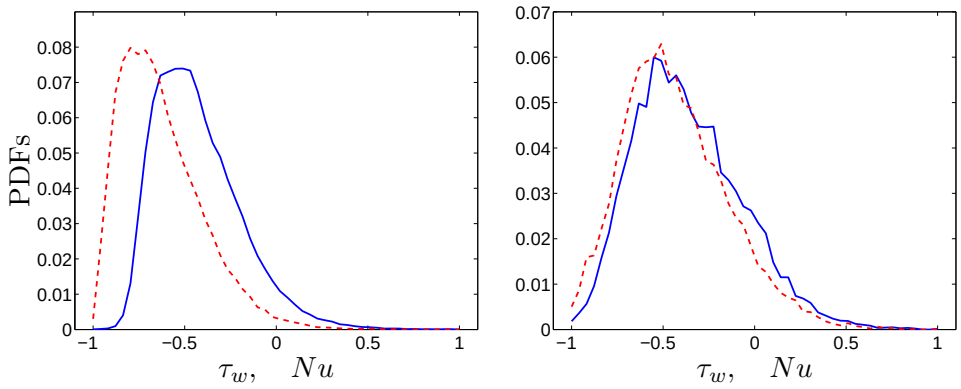

(a) DNS, $Re = 150$.

(b) Hybrid LES-RANS, $Re = 4000$.

Figure 7: Channel flow. Probability functions of wall heat transfer and wall shear stress. —— : shear; - - - : heat transfer.

heat transfer decrease with increasing Reynolds number, although the opposite trend is seen in the peak values of all resolved fluctuations. Also from DNS of channel flows it is known that the turbulent normal stresses increase with increasing friction Reynolds number. In the present study the accuracy of the DNS simulations is consider to be good. In the hybrid LES-RANS simulations, it may be that the URANS model dampens the resolved fluctuations too much, yielding too small fluctuating wall heat transfer and wall shear stress.

Another way to look at the fluctuating wall heat transfer and wall shear stress is to evaluate the probability density functions, the PDFs. They are shown in Fig. 7. They have been normalized so that τ_w' and Nu' vary between -1 and $+1$. First it can be seen that both τ_w' and Nu' are not symmetric around their mean; they are biased (i.e. their skewness is non-zero) in the sense that values that are lower than the mean are more common than those larger than the mean, but that on the other hand the largest fluctuations are those which are larger than the mean. For $Re_\tau = 150$, the skewness is larger for the heat transfer than for the shear stress, whereas for $Re_\tau = 4000$ the skewness is the same for both quantities. Again, the hybrid LES-RANS results cannot be fully trusted (although they may be correct). The skewness

$$S_q = \frac{\langle q_w'^3 \rangle}{q_{w,RMS}'^{1.5}} \tag{5}$$

for wall heat transfer is 1.06 and 0.65 for $Re_\tau = 150$ and 4000, respectively. The corresponding numbers are 0.97 and 0.60 for the wall shear stresses.

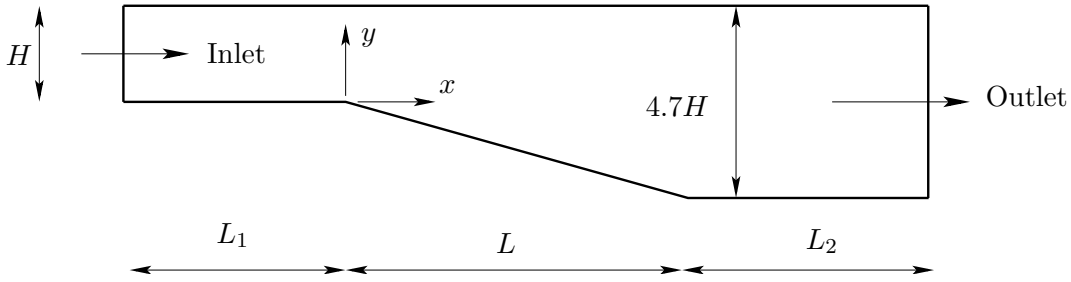

Figure 8: Plane asymmetric diffuser (not to scale). $L_1 = 7.9H$, $L = 21H$, $L_2 = 28H$. The spanwise width is $z_{max} = 4H$. The origin of $x - y - z$ is at the lower wall at the entrance of the diffuser.

3.2 Diffuser Flow Simulations.

The configuration is an asymmetric plane diffuser, see Fig. 8, with Reynolds number $Re = U_{b,in}H/\nu = 18\,000$ ($U_{b,in} = H = 1$). The opening angle is 10^o. Instantaneous inlet boundary conditions are prescribed from synthetic boundary conditions Davidson (2007) and convective boundary conditions are used at the outlet. The temperature is set to 0 at the lower wall and equal to 1 at the upper wall. At the inlet the temperature profile is taken from fully developed channel flow with the same boundary boundary conditions at the walls. The inlet conditions are obtained from a 1D RANS simulation using the $k-\omega$-SST model. Periodic boundary conditions are prescribed in the spanwise direction. The mesh has $256\times64\times32$ (x, y, z) cells (body-fitted, structured, nearly orthogonal mesh), which gives a spanwise resolution at the inlet of $\Delta z^+ \simeq 120$.

Figure 9 presents the velocity profiles. The agreement is good. The peak in the region $14H < x < 20H$ is slightly under-predicted. Furthermore, it can be seen that at $x = 6H$ the peak velocity is slightly over-predicted and consequently the separation is predicted too early.

In Fig. 10 the velocity profiles computed with pure LES with a one-equation SGS model are presented. The velocity profiles in the entrance of the diffuser are very poor. However, further downstream the LES-results agree well with experiments, but this must be regarded as purely coincidental, considering the very poor predictions further upstream.

The predicted pressure coefficients in Fig. 11a are in rather good agreement with experiments in the first part of the expansion. Further downstream the predicted C_p is too large. Also the pressure coefficient predicted in Kaltenbach *et al.* (1999) is in this region slightly higher than the experimental values (but smaller than the present predictions). It is suggested in Kaltenbach *et al.* (1999) that part of the discrepancy can be attributed to three-dimensional effects in the middle part of the expansion, giving bulk velocities in the center plane which are some 5% too high.

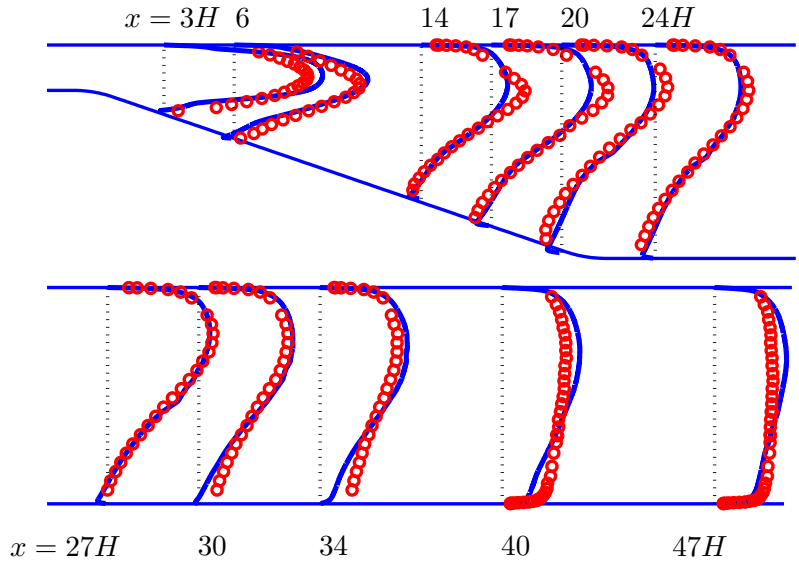

Figure 9: Diffuser flow. $\langle \bar{U} \rangle / U_{b,in}$ profiles. Lines: hybrid LES-RANS; markers: experiments Buice & Eaton (1997)

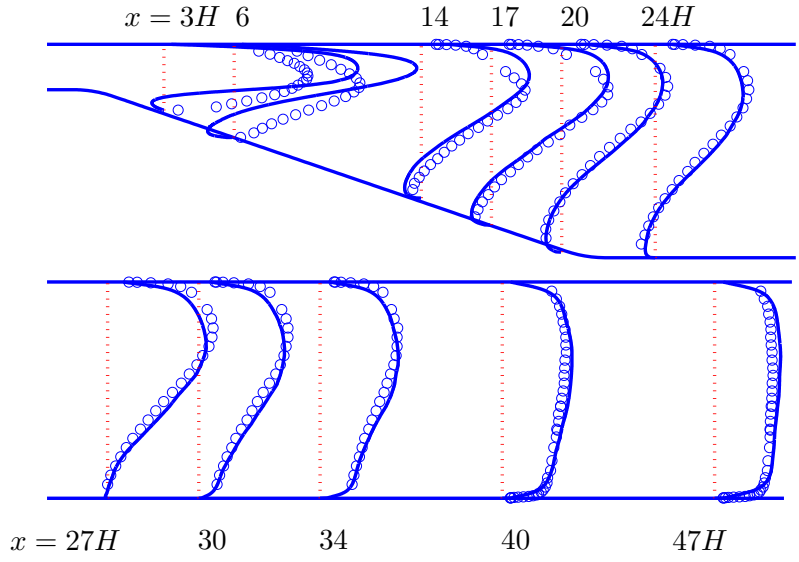

Figure 10: Diffuser flow. $\langle \bar{U} \rangle / U_{b,in}$ profiles. LES with a one-equation k_{sgs} model.Solid lines: LES; markers: experiments Buice & Eaton (1997)

Figure 11b shows that the predicted recirculation region along the lower wall is too strong compared with experiments. The predicted skin friction goes negative at $x/H = 1.5$ and assumes positive value at $x/H \simeq 32.5$. For $x/H > 20$, the predicted skin friction along the lower wall agrees well with experiments. At the upper wall the predicted skin friction agrees fairly well

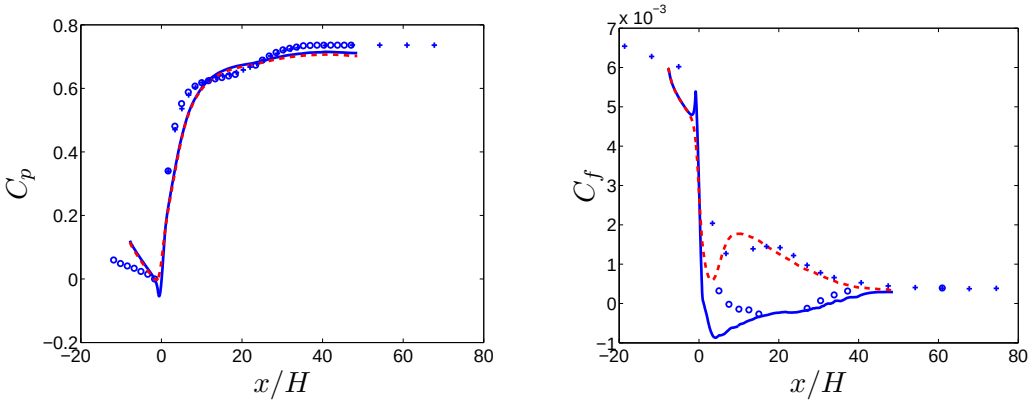

(a) Pressure coefficient.

(b) Friction coefficient.

Figure 11: Diffuser flow. Pressure and skin coefficients. —— wall; - - - : upper wall; markers: experiments Buice & Eaton (1997).

except at the start of the expansion.

The predicted shear stresses, both resolved and modelled, are compared with experiments in Fig. 12. In the beginning of the expansion the predicted stresses near the lower wall are much too large. The magnitude of the modelled shear stresses at $x/H = 3$ and $x/H = 6$ is similar to that in the experiments, but the resolved stresses are approximately twice as large as the experimental values. It may seem somewhat surprising that the predicted shear stresses are that different from the experimental ones, and still the agreement between the predicted and velocities is that good. The reason is that in regions where the resolved stress is large, it is not a dominating term. For example at $x/H = 3$, at the y location of maximum shear stress the advective term $\langle\bar{U}\rangle\partial\langle\bar{U}\rangle/\partial x$ is three times larger than the y-gradient of the resolved shear stress and the magnitude of the pressure gradient $\partial\bar{P}/\partial x$ is similar to that of $-\partial\langle u'v'\rangle/\partial y$. From $x/H = 13$ and downstream the agreement between predicted and experimental shear stresses is much better.

Greater detail can be found in Davidson & Dahlström (2005).

3.2.1 Heat transfer

The temperature profiles are shown in Fig. 13. In the part of the flow where the flow corresponds to fully developed channel flow, the temperature profiles are rather flat, but that changes in the diffuser part where the cross-stream gradient in the central part of the flow is non-negligible.

Figure 14 presents the vertical heat flux, both the resolved, $\langle v't'\rangle$ and the modelled, $-\langle\nu_t/Pt_t\partial\bar{T}/\partial y\rangle$. In the fully developed regions where the advective terms are negligible, the balance of the temperature equation re-

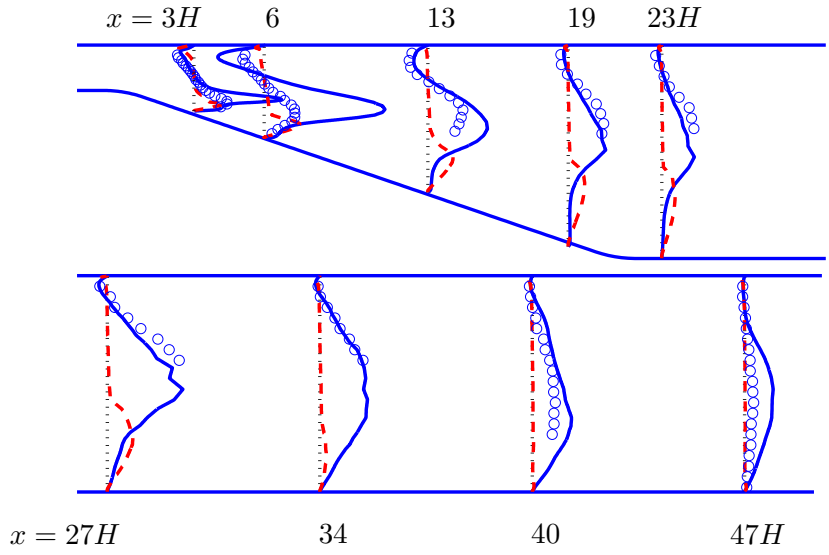

Figure 12: Diffuser flow. Profiles of turbulent shear stresses. —— : resolved $\langle -u'v' \rangle / U_{b,in}^2$; - - - - : modelled $2\langle \nu_t \bar{S}_{12} \rangle / U_{b,in}^2$. The lower profiles have been multiplied by two.

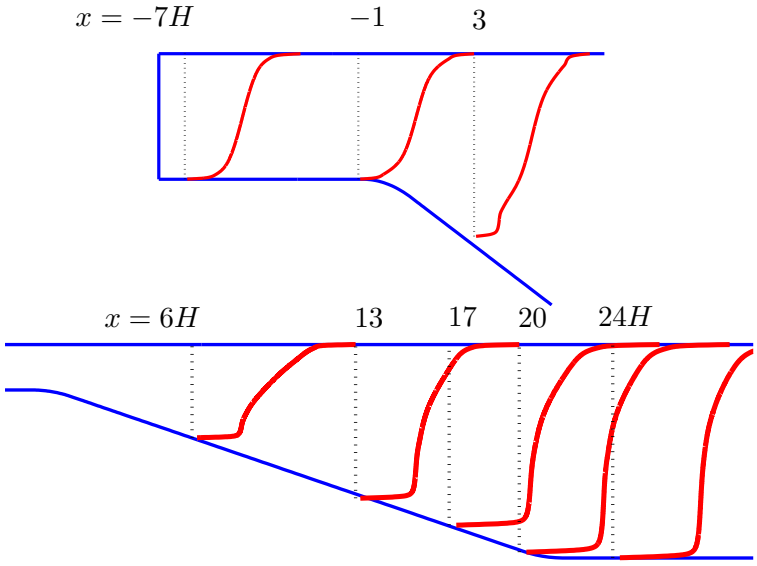

Figure 13: Diffuser flow. Profiles of mean temperature, $\langle \bar{T} \rangle$.

duces to Eq. 2. This balance should be approximately be satisfied in the channel part upstream the throat (i.e. for $x < 0$) and far downstream of the diffuser part. This balance seems to be satisfied at $x = -H$. Near the inlet, at $x = -7H$, it is not satisfied, and the reason is that the prescribed mean inlet temperature profile undergoes a change near the inlet so that the advective terms come into play. Furthermore, it can be seen that the

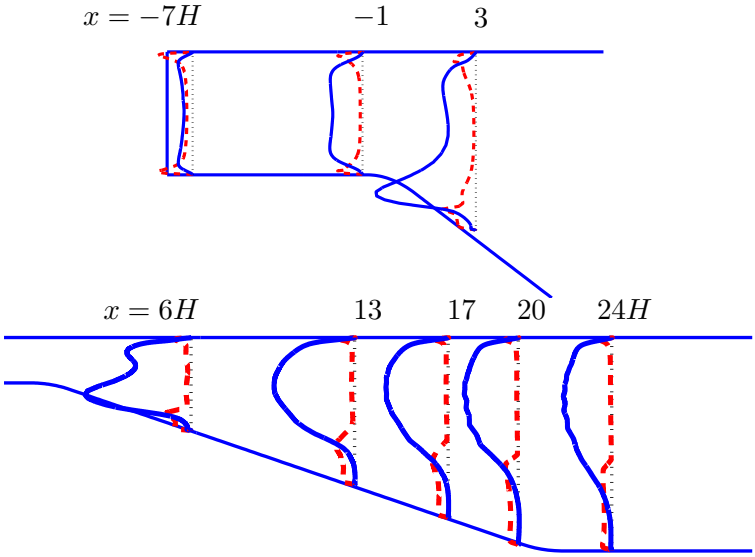

Figure 14: Diffuser flow. Profiles of turbulent heat fluxes. —— : resolved $\langle v't' \rangle$; - - - : modelled $\langle -\nu_t \partial \bar{T}/\partial y \rangle$.

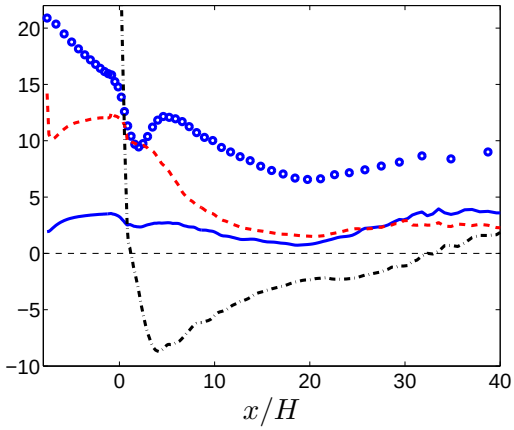

Figure 15: Diffuser flow. —— : Nu'_{RMS}; - - - : $10\,000 \cdot c'_{f,RMS}$; - · - : $10\,000 \cdot c_f$; ○: Nu.

resolved heat flux in the upper half of the diffuser is much larger than the modelled heat flux. The reason is that in the lower part the equations are in URANS mode (i.e. in the URANS region) Davidson & Dahlström (2005).

In Fig. 15 the skin-friction, the Nusselt number and their RMS fluctuations are presented. The skin-friction is formed with the inlet bulk velocity and the Nusselt number is formed with the channel height at the inlet and the temperature difference between the walls. These are the quantities that are the most interesting for an engineer: the loss and the heat transfer (both their mean and RMS quantities). From the skin-friction it is seen that the

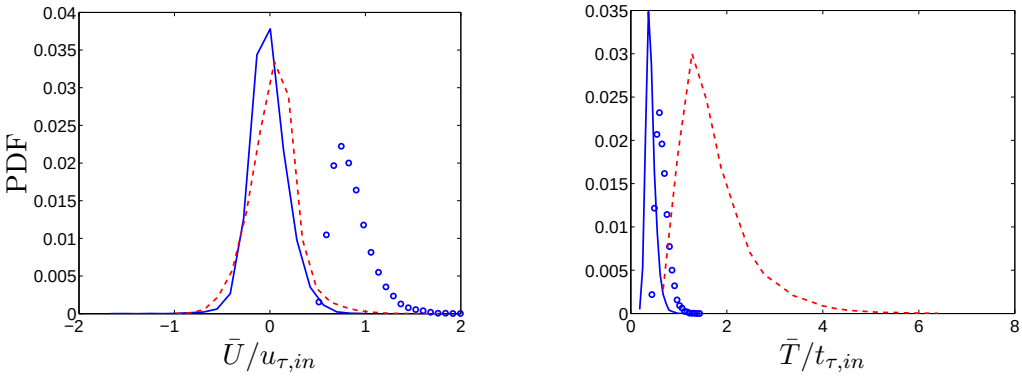

(a) Velocity. (b) Temperature.

Figure 16: Diffuser flow. Probability function of wall shear and heat transfer at lower wall. —— $x = 1.4H$ (near separation point); - - - : $x = 33H$ (near re-attachment point); ○: $x = -3H$.

separation takes place at $x \simeq 3H$ and that the re-attachment occurs at $x \simeq 31H$. Both the skin-friction and the Nusselt number are largest in the channel part upstream of the diffuser. The Nusselt number stays fairly large in the entire diffuser and reaches a local maximum near the reattachment point. This has also been seen in, for example, backstep-facing flow Vogel & Eaton (1985); Labbé *et al.* (2002). The fluctuations of the skin-friction is also large in the channel part ($x < 0$). But the RMS of the Nusselt number is largest just downstream of the re-attachment point, where Nu_{RMS}/Nu reaches 45%. It can be seen in Fig. 15 that there is no relation between the skin-friction and the Nusselt number. The skin-friction is, as argued by Vogel & Eaton (1985), governed by the mean flow whereas the wall heat transfer seems to be dictated by the turbulence.

It is interesting to study the instantaneous resolved skin-friction and Nusselt number. Figure 16 presents the probability density functions of the near-wall wall-parallel velocity and temperature (which are proportional to the skin-friction and the Nusselt number, respectively) at three stations: in the channel part upstream of the diffuser, near the separation point and near the reattachment point. The form of the PDF of the skin-friction is rather similar for all three positions; its mean varies of course according to Fig. 15 (it is large in the channel part whereas it is close to zero near the separation and reattachment points). However, the PDF for the Nusselt number is very different at the reattachment point compared to the two other locations. Near the reattachment the fluctuations of the Nusselt are very large. This is quantified by the skewness (see Eq. 5) which takes the values $3.0, 3.2, 3.9$ (the three positions from upstream to downstream). The

corresponding numbers for the wall shear stress are 3.2, −0.15 and 2.10.

4 Discussion

Heat transfer predictions using unsteady simulations have been presented. First, two channel flows were simulated. DNS was used at low Reynolds number ($Re_\tau = 150$) and hybrid LES-RANS was used at high Reynolds number ($Re_\tau = 4000$). The former results are considered to be of high accuracy and the latter are fairly accurate for the mean fluid flow. The Nusselt number given by experimental correlations is some 50% larger than the predicted values for both Reynolds numbers. However, the agreement for the ratio of the $Re_\tau = 150$-case to the $Re_\tau = 4000$-case is fairly good between experimental correlations and simulations.

The fluid flow and heat transfer in an asymmetric diffuser were also studied in this report. Hybrid LES-RANS is used and the agreement for the flow fluid is fairly good. However, it should be pointed out that the predicted results *are* dependent on how the matching plane between LES and URANS is defined. Furthermore, LES fails completely for this flow. For more details on the fluid flow simulations, see Davidson & Dahlström (2005). The temperature field is also predicted for this case although no experimental data exist. The object was to study a heat transfer case which includes recirculating flow and for which the fluid flow is (fairly) well predicted.

For both the channel flow and the diffuser flow it is found that the fluctuating wall heat transfer is of comparable magnitude or larger than the fluctuating wall shear stress. In the recirculating region in the diffuser flow both the mean and the fluctuating Nusselt number are large whereas both the skin-friction and its fluctuations are small.

Probability functions of the wall shear stress and the Nusselt number are also studied for both flows. Although, the fluctuations of the wall shear stress in channel flow are slightly larger than those of the Nusselt number, the skewness of the Nusselt number is larger than that of the wall shear stress. This means that the extreme values are larger for the Nusselt number than for the shear stress. This is even more pronounced near the reattachment point in the diffuser flow, where both the RMS of the Nusselt number and its skewness are very large. This is interesting since large temperature fluctuations may cause thermal fatigue and crack fatigue crack initiation and propagation which eventually may lead to structural failure.

Can the wall heat transfer predicted by hybrid LES-RANS be trusted? It is certainly much more accurate than standard RANS or coarse LES. In the former case no resolved fluctuations are resolved but all turbulence is modelled leading to poor accuracy. Unsteady RANS (URANS) should be more accurate, possibly as accurate as hybrid LES-RANS. Well-resolved LES is always accurate, but at high Reynolds number it is not affordable;

a coarse LES is less accurate than hybrid LES-RANS and URANS. The main weakness of hybrid LES-RANS and URANS is probably the very fact that URANS is employed in the near-wall region. Hence a large part of the turbulence in the near-wall region is modelled and the resolved turbulence is dampened by large turbulent viscosities. This may be a more important weakness for the predicted heat transfer than for the predicted skin-friction since – as has been seen in this work – the fluctuations of the wall heat transfer are larger than those of the skin-friction. New wall models for heat transfer are probably needed.

References

Buice, C. & Eaton, J. 1997 Experimental investigation of flow through an asymmetric plane diffuser. Report No. TSD-107. Thermosciences Division, Department of Mechanical Engineering, Stanford University, Stanford, California 94305.

Davidson, L. 2007 Using isotropic synthetic fluctuations as inlet boundary conditions for unsteady simulations. *Advances and Applications in Fluid Mechanics* **1** (1), 1–35.

Davidson, L. & Billson, M. 2006 Hybrid LES/RANS using synthesized turbulence for forcing at the interface. *International Journal of Heat and Fluid Flow* **27** (6), 1028–1042.

Davidson, L., Čuturić, D. & Peng, S.-H. 2003 DNS in a plane vertical channel with and without buoyancy. In *Turbulence Heat and Mass Transfer 4* (ed. K. Hanjalić, Y. Nagano & M. Tummers), pp. 401–408. New York, Wallingford (UK): begell house, inc.

Davidson, L. & Dahlström, S. 2005 Hybrid LES-RANS: An approach to make LES applicable at high Reynolds number. *International Journal of Computational Fluid Dynamics* **19** (6), 415–427.

Davidson, L. & Peng, S.-H. 2003 Hybrid LES-RANS: A one-equation SGS model combined with a $k-\omega$ model for predicting recirculating flows. *International Journal for Numerical Methods in Fluids* **43**, 1003–1018.

Emvin, P. 1997 The full multigrid method applied to turbulent flow in ventilated enclosures using structured and unstructured grids. PhD thesis, Dept. of Thermo and Fluid Dynamics, Chalmers University of Technology, Göteborg.

Incropera, F. & DeWitt, D. 1996 *Fundamentals of Heat and Mass Transfer*, 4th edn. New York: John Wiley & Sons.

Kaltenbach, H., Fatica, M., Mittal, R., Lund, T. & Moin, P. 1999 Study of flow in plane asymmetric diffuser using large-eddy simulation. *Journal of Fluid Mechanics* **390**, 151 – 186.

Labbé, O., Montreuil, E. & Sagaut, P. 2002 Large eddy simulation of heat transfer over a backward-facing step. *Numerical Heat Transfer. Part A* **42**, 73–90.

Moser, R., Kim, J. & Mansour, N. 1999 Direct numerical simulation of turbulent channel flow up to $Re_\tau = 590$. *Physics of Fluids A* **11**, 943–945.

Vogel, J. & Eaton, J. 1985 Combined heat transfer and fluid dynamic measurements downstream a backward-facing step. *Journal of Heat Transfer* **107**, 922–929.